A marginal band of microtubules transports and organizes mitochondria in retinal bipolar synaptic terminals

Malkolm Graffe,[1] David Zenisek,[2] and Justin W. Taraska[1]

[1]National Heart Lung and Blood Institute, National Institutes of Health, Bethesda, MD 20892
[2]Department of Cellular and Molecular Physiology, Yale University School of Medicine, New Haven, CT 06510

A set of bipolar cells in the retina of goldfish contains giant synaptic terminals that can be over 10 µm in diameter. Hundreds of thousands of synaptic vesicles fill these terminals and engage in continuous rounds of exocytosis. How the cytoskeleton and other organelles in these neurons are organized to control synaptic activity is unknown. Here, we used 3-D fluorescence and 3-D electron microscopy to visualize the complex subcellular architecture of these terminals. We discovered a thick band of microtubules that emerged from the axon to loop around the terminal periphery throughout the presynaptic space. This previously unknown microtubule structure associated with a substantial population of mitochondria in the synaptic terminal. Drugs that inhibit microtubule-based kinesin motors led to accumulation of mitochondria in the axon. We conclude that this prominent microtubule band is crucial to the transport and localization of mitochondria into the presynaptic space to provide the sustained energy necessary for continuous transmitter release in these giant synaptic terminals.

The Journal of General Physiology

INTRODUCTION

Neurons are some of the most morphologically complex cells in the body. This complexity is seen in their overall shape as well as in the spatial distribution of their molecules and organelles. The specific architecture and internal organization of a neuron influence their fundamental signaling behavior. This relationship between form and function is particularly evident in the retina, where multiple steps in visual processing occur between discrete layers of interconnected but morphologically distinct cell types (Masland, 2012). How a neuron's internal molecular structure is spatially organized and how this organization is maintained are not clear. Understanding these structures is critical to understanding how neurons, neural circuits, and the nervous system function as a whole.

Bipolar cells of the retina are small interneurons that transmit information from the outer retina to the inner retina mostly without the benefit of action potentials (Masland, 2012). Bipolar cells receive input directly from photoreceptors and propagate these signals by graded changes in their continuous rates of exocytosis. This sequential information processing across several cell types in the retina is how visual information is processed by the circuit. In some fish species, such as goldfish (*Carassius auratus*) and zebrafish (*Danio rerio*), a subset of bipolar cells has giant presynaptic terminals that can be upwards of 10 µm in diameter at the end of a short axon (Stell, 1967). The large size and experimental accessibility of these terminals have made them an important model system for electrophysiology and imaging of vertebrate synapses (Tachibana and Kaneko, 1987; Lagnado et al., 1996; von Gersdorff et al., 1996, 1998; Zenisek et al., 2000). Bipolar terminals are also characterized by having dozens of submicron-sized synaptic ribbons that position a population of synaptic vesicles close to the plasma membrane (Lagnado, 2003). Synaptic ribbons are common to other sensory neurons including photoreceptors and hair cells in the auditory and vestibular systems (Matthews and Fuchs, 2010).

A comprehensive view of the internal spatial organization of bipolar cells has been lacking. Here, we used 3-D fluorescence and 3-D electron microscopy to determine the subcellular structure of individual retinal bipolar terminals. We discovered a prominent marginal band of microtubules that emerges from the axon and formed a distinctive loop that traversed the terminal close to the plasma membrane. This loop is similar in structure to the marginal band of microtubules found in red blood cells (Lazarides, 1987). This microtubule band contained multiple posttranslational modifications and was present in both isolated cells and cells within intact retinal tissue. We found that ribbons were not specifically associated with the microtubule band in the terminal. Mitochondria, however, appeared to be associated with these microtubules. In living cells, mitochondria could be observed to move along microtubule

Correspondence to Justin W. Taraska: justin.taraska@nih.gov

Abbreviations used in this paper: IPL, inner plexiform layer; TEM, transmission electron microscopy; TMRM, tetramethyl rhodamine methyl ester.

The Rockefeller University Press $30.00
J. Gen. Physiol. Vol. 146 No. 1 109–117
www.jgp.org/cgi/doi/10.1085/jgp.201511396

tracks, and drugs that inhibit microtubule-based kinesin motors stalled mitochondria and induced prominent swellings of the axon. We propose that this distinctive microtubule structure could help transport and localize mitochondria and other presynaptic organelles within the giant terminal of retinal bipolar cells to supply these continuously active giant terminals with their large ATP requirements and distribute other organelles throughout the synaptic cytoplasmic space.

MATERIALS AND METHODS

Cells

Isolated goldfish bipolar cells were prepared as described previously (Heidelberger and Matthews, 1992). Specifically, goldfish (~5–7 cm in length) were dark adapted for 30 min before euthanasia by cervical decapitation and pithing. In ambient light, eyes were removed with curved forceps and immediately placed into oxygenated saline buffer (mM): 120 NaCl, 2.5 KCl, 1 $MgCl_2$, 0.5 $CaCl_2$, 10 HEPES, and 10 glucose, with pH adjusted to 7.4 with NaOH. Retinas were manually removed and washed with saline buffer. Retinas were incubated in saline buffer with papain (30 units/ml; Sigma-Aldrich) and 2.7 mM cysteine for 30 min. Retinas were made into a cell suspension by manual trituration through a narrowed flamed glass pipette in saline buffer and plated onto cleaned cover glass (25-mm round; no. 1.5; Warner Instruments). The cell suspension was allowed to settle for 3–10 min. The suspension was then removed, and adherent cells were carefully washed with saline buffer. Bipolar neurons were identified by their distinct morphology (Fig. 1 A).

Immunofluorescence

Cells were fixed with 4% paraformaldehyde in PBS for 50 min and permeabilized with 0.5% Triton X-100 (Sigma-Aldrich), 3% BSA (Thermo Fisher Scientific), and 10% goat serum (Gibco) in PBS for 3 min at room temperature (RT). Cells were blocked with 0.2% Triton X-100, 3% BSA, and 10% goat serum in PBS for 60 min and incubated in primary antibody (1:200) in blocking buffer overnight at RT. Cells were washed with blocking buffer for 20 min and incubated in secondary antibody (1:1,000) for 40 min at RT. Secondary antibody was removed, and coverslips were washed with blocking buffer for 20 min. Slices of goldfish retina were prepared by fixing whole retina in 4% paraformaldehyde for 2 h followed by embedding in 3% low melting point agarose in PBS. 100-µm slices were made with a Vibratome 3000 (Leica). Slices were immunostained as described above. Stained slices were placed in Secure-Seal imaging spacers (0.12-mm depth; Grace Bio-Labs) in Vectashield H-1000 mounting medium (Vector Laboratories) and mounted for imaging on square glass coverslips (no. 1.5; Warner Instruments) and slides. The following antibodies were used at a 1:200 dilution: mouse anti–α-tubulin (ab7291; Abcam), rabbit anti–α-tubulin (ab4047; Abcam), mouse anti-acetylated α-tubulin ([6-11B-1]; ab24610; Abcam), mouse anti-polyglutamylated α-tubulin ([B3]; ab11324; Abcam), and mouse anti-tyrosinated α-tubulin (T9028; Sigma-Aldrich); mouse anti-CtBP ([B-3]; sc-55502; Santa Cruz); and rabbit anti-PKCα ([Y124]; ab32376; Abcam). The following secondary antibodies were used at a 1:1,000 dilution: Alexa Fluor 488 goat anti–mouse IgG (H+L; Invitrogen) and Alexa Fluor 647 goat anti–rabbit IgG (H+L; Invitrogen).

Live cell imaging and analysis

Cells were incubated in saline buffer with SiR-tubulin or SiR-actin (2 ng/ml; provided by K. Johnsson, EPFL, Lausanne, Switzerland, and Spirochrome Ltd., Stein am Rhein, Switzerland) for 10 min. Cells were washed with saline buffer and imaged for up to 2 h. For dual staining of mitochondria and microtubules, cells were first stained with SiR-tubulin and then incubated with 1 ng/ml tetramethyl rhodamine methyl ester (TMRM; Invitrogen) for 30 s. Next, cells were washed and imaged for up to 1 h.

Osmotic shock experiments were performed on dissociated cells firmly attached to coverslips with hyperosmotic buffer (400 mM sucrose added to saline buffer) or hypoosmotic buffer (1:1 dilution of saline buffer and water). Images were collected every 2 min, and buffers were exchanged every 10 min, alternating between isoosmotic and hyperosmotic or hypoosmotic buffers. For microtubule depolymerization experiments, cells were incubated in KaryoMAX colcemid solution (Life Technologies) in 10 µg/ml HBSS (Sigma-Aldrich) diluted at 1:50 in saline buffer and in combretastatin A-4 (Life Technologies) in saline buffer for 20 min or 50 µM nocodazole (Sigma-Aldrich) for 30 min. For high potassium stimulation, cells were incubated with saline solution containing 50 mM K^+ (isoosmotic replacement with NaCl) and 2.5 mM $CaCl_2$. Cells were imaged every 2 min for a total of 6 min (Job and Lagnado, 1998). For aurintricarboxylic acid (Sigma-Aldrich) treatment, cells were incubated with 10 µM of the drug in saline buffer.

3-D confocal images were taken on a confocal microscope (LSM 780; Carl Zeiss) with a 40× objective (NA = 1.4) with 0.36-µm z-step intervals. The following laser lines were used for excitation: 488 nm, Alexa Fluor 488; 561 nm, TMRM; 641 nm, Alexa Fluor 647, SiR-actin, and SiR-tubulin. A transmitted light image was also collected during each acquisition. Colocalization between the two 3-D confocal image stack channels was quantified in MATLAB (MathWorks) using a Pearson's correlation coefficient as described previously for each slice and averaged across the terminal (Larson et al., 2014).

Block-face serial SEM

For serial block-face SEM imaging, whole retinas were fixed in a mixture of 2.5% glutaraldehyde and 2% formaldehyde in sodium cacodylate buffer with 2 mM calcium chloride at RT for 5 min, and then on ice for an additional 2–3 h. Fixed retinas were stained with osmium tetroxide and uranyl acetate, and mounted and stained with lead aspartate for serial 3-D SEM as described previously (Pfeifer et al., 2015). The trimmed, resin-embedded stained blocks were imaged using a 3View serial block-face imaging system (Gatan) installed on a SIGMA-VP (variable pressure; Carl Zeiss) SEM, operating at an accelerating voltage of 1.5 kV using a standard 30-µm condenser aperture. The SEM was operated in high vacuum. Data were collected with a pixel size of 5.75 nm in the x–y plane and 25 nm along the z axis. Individual block-face electron micrographs were locally aligned with IMOD software (Kremer et al., 1996). The synaptic terminals of bipolar cells were recognized in the inner plexiform layer (IPL) by the presence of synaptic ribbons, vesicles, mitochondria, and their distinct morphology. Full 3-D reconstructions of the two bipolar terminals were made by two blind users by hand segmentation of the plasma membrane, ribbons, mitochondria, and microtubule structures of the individual serial images in Amira software (FEI) and TrakEM2 software (FIJI).

Transmission electron microscopy (TEM)

For TEM, goldfish retinas were fixed in cacodylate buffer with 2.5% glutaraldehyde, 1% paraformaldehyde, and 120 mM NaCl, pH 7.4. Fixed retinas were washed in cacodylate buffer, post-fixed with 1% OsO_4 in cacodylate buffer, stained en bloc with uranyl acetate, ethanol dehydrated, and embedded in EMbed 812. 60-nm cross sections were prepared and stained with uranyl acetate and lead citrate before imaging with an electron microscope (JEM1400; JEOL USA, Inc.) equipped with a digital camera (AMT XR-111; Advanced Microscopy Techniques, Corp.).

RESULTS

The cytoskeleton is the primary underlying support structure for eukaryotic cells. To image the structure of the cytoskeleton of giant synaptic terminals of bipolar cells, we first used a live cell stain for microtubule filaments, SiR-tubulin (Lukinavičius et al., 2014). Fig. 1 shows a single living retinal bipolar cell imaged with white light (Fig. 1 A) and stained with SiR-tubulin (Fig. 1 B). SiR-tubulin crosses the plasma membrane and stains microtubules in living cells and tissue (Lukinavičius et al., 2014). After the addition of the dye, distinct microtubules could be seen throughout the cell body and axon of the cell. Unexpectedly, in almost every visible bipolar cell in our cultures, we discovered a large distinctive marginal band of microtubules that extended down from the axon and entered the synaptic terminal. This microtubule structure formed an extended loop reminiscent of the marginal band of microtubules found in red blood cells (Behnke, 1970; Lazarides, 1987). Fig. 1 C shows a panel of five synaptic terminals to illustrate the structural diversity and architecture of the microtubule band found inside these terminals. Microtubule bands were occasionally seen to twist, buckle, and hook. Fig. 1 D shows that these structures were also stained and visible with antibodies raised against microtubules in fixed cells. Similar structures were seen in bipolar cells isolated from zebrafish retina and stained with SiR-tubulin (not depicted). One of the distinguishing characteristics of these neurons is the numerous ribbons that populate the synaptic terminal. Using antibody against CtBP, which stains synaptic ribbons, we detected no obvious association of ribbons with microtubules by 3-D confocal microscopy (Fig. 1 E) (Schmitz et al., 2000; Zenisek et al., 2004). Bipolar terminals had an average of 24 ± 1 ribbons/cell (n = 40 cells). These numbers, although slightly lower than past estimates, are consistent with previous measurements of ribbon densities in these cells (von Gersdorff et al., 1996, 1998; Holt et al., 2004; Zenisek et al., 2004). Actin staining with the live cell actin-specific SiR-actin probe indicated that unlike microtubules, actin was distributed throughout the terminal (Fig. 2, A–C, example cell; n = 8 cells) (Lukinavičius et al., 2014).

In mature neurons, microtubules undergo extensive posttranslational modifications, including acetylation, tyrosination, and poly-glutamylation (Magiera and Janke, 2014). These modifications are proposed to regulate

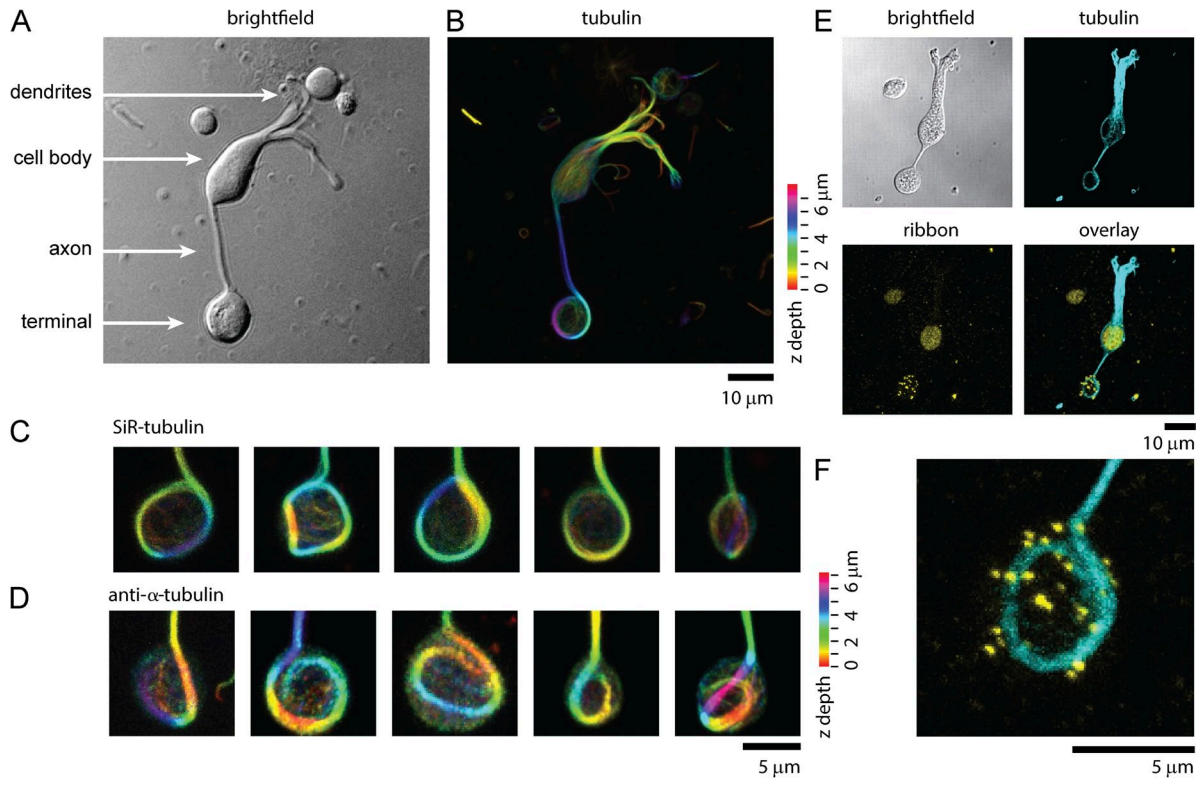

Figure 1. A marginal band of microtubules in retinal bipolar synaptic terminals. (A) White light image of a single isolated retinal bipolar cell. (B) 3-D max intensity projection of SiR-tubulin staining of the same cell shown in A. Color code represents Z-height. (C) Gallery of five different synaptic terminals stained with SiR-tubulin. Color code represents Z-height. (D) Five representative terminals stained with anti–α-tubulin antibody. Color code represents Z-height. (E) Single bipolar cell imaged with bright field with the 3-D max intensity projection of fluorescence of anti-tubulin antibody (cyan), an antibody that recognizes ribbons (yellow), and the overlay of both fluorescent images. (F) A magnified view of the synaptic terminal shown in E.

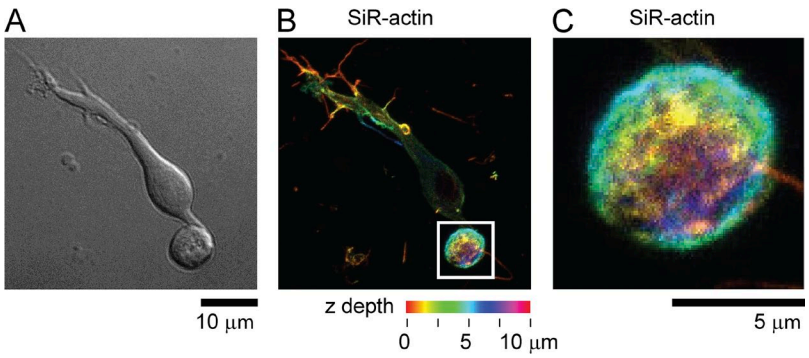

Figure 2. Actin is distributed throughout the synaptic terminal in retinal bipolar cells. (A) White light image and (B) 3-D max intensity projection of SiR-actin staining of a goldfish retinal bipolar cell. Spectrum represents Z-height. (C) Magnified view of region shown in the white box in B.

the biophysical properties of microtubules, including their stability and interactions with proteins such as motors (Magiera and Janke, 2014). To investigate whether the microtubule loop in bipolar cells contains posttranslation modifications, we stained bipolar cells with antibodies that recognize three different tubulin posttranslational modifications. Fig. 3 shows that the microtubules found in the dendrites, cell body, axon, and terminal of bipolar neurons contain all three modifications we examined. Of note, the large microtubule loop found in the synaptic terminal contained each of these three modifications. Quantitative analysis indicated that the average fluorescence intensity ratio of the modified tubulin to α-tubulin signal was consistently

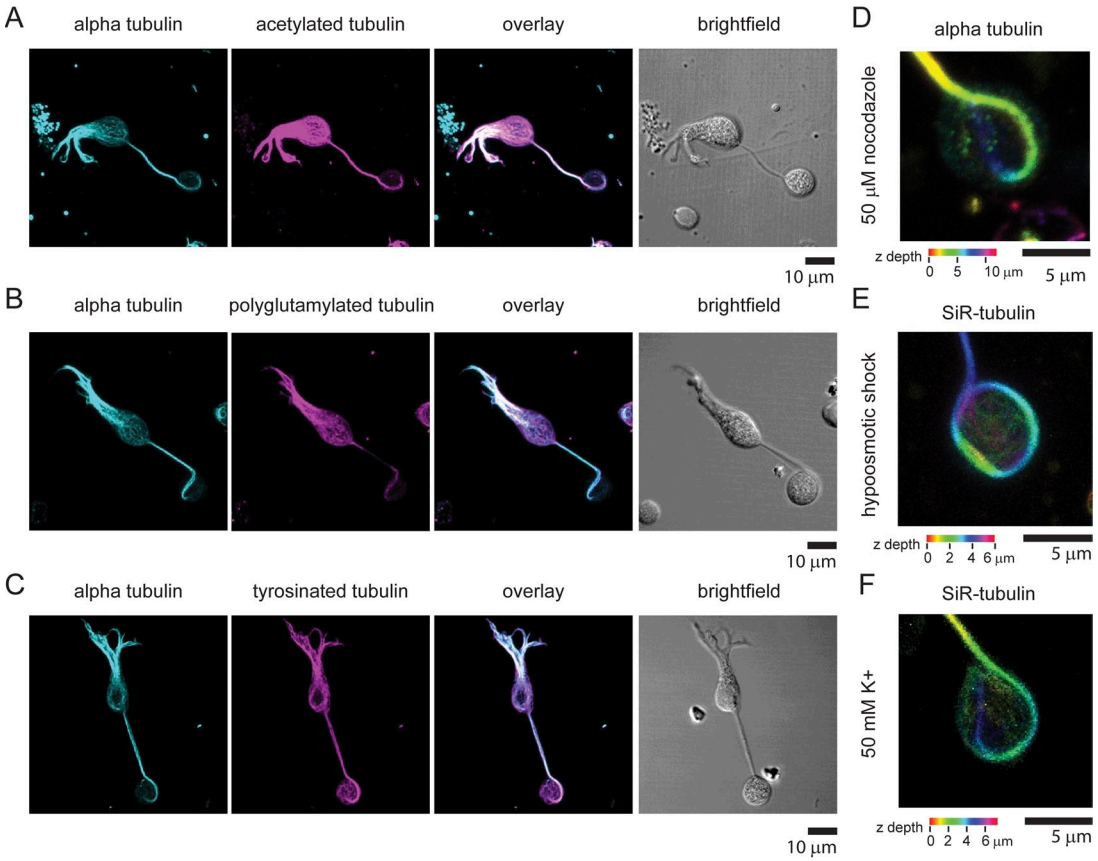

Figure 3. Marginal band of microtubules in retinal bipolar synapses contains posttranslational modifications. (A) 3-D max intensity projection of a single bipolar cell stained with anti-tubulin antibody and an antibody that recognizes acetylated tubulin. The overlay of both fluorescent images and a white light image are also shown. (B) 3-D max intensity projection of a single bipolar cell stained with anti-tubulin antibody and an antibody that recognizes polyglutamylated tubulin. The overlay of both fluorescent images and a white light image are shown to the right. (C) 3-D max intensity projection of a single bipolar cell stained with anti-tubulin antibody and an antibody that recognizes tyrosinated tubulin. The overlay of both fluorescent images and a white light image are shown to the right. (D) Image of a representative synaptic terminal stained with anti-tubulin treated with 50 μM nocodazole for 30 min. (E) Image of a representative synaptic terminal stained with SiR-tubulin–treated hypoosmotic buffer for 6 min. (F) Image of a representative synaptic terminal stained with SiR-tubulin depolarized with a high K^+ extracellular buffer for 6 min.

higher in the synaptic terminal than in the cell body (enrichment: acetylated tubulin, 40% ± 04 SEM%, $n = 7$ cells; polyglutamylated tubulin, 98% ± 14 SEM %, $n = 5$ cells; tyrosinated tubulin, 98% ± 21 SEM %, $n = 8$ cells). These data indicate that these microtubule modifications were slightly enriched in the marginal band microtubules compared with those microtubules found in the cell body. These data suggest that the microtubules throughout these neurons and particularly those found in the synaptic terminal are extremely stable. To test this hypothesis, we treated cells with 50 µM of the microtubule depolymerizing agent nocodazole and found that the microtubule loop was still present in the terminal after drug treatment ($n = 15$ cells; example terminal shown in Fig. 3 D). Furthermore, the microtubule loop was also present after cell swelling by hypoosmotic shock ($n = 8$ cells; example terminal shown in Fig. 3 E) and high potassium stimulation ($n = 9$ cells; example terminal shown in Fig. 3 F) (Heidelberger and Matthews, 1992; Job and Lagnado, 1998). These data suggest that this structure constitutes a stable architectural feature of these cells and is not highly dynamic.

The above data were generated from isolated cells. We next asked whether the same microtubule structure could be observed in retinal tissue by making slices of intact goldfish retina. In these slices, we could readily observe a population of PKCα-positive cells with cell bodies located in the inner nuclear layer with giant terminals in the IPL where they form synapses (Fig. 4 A). The morphology of these bipolar cells was similar to previous staining on goldfish retina with PKC antibodies (Job and Lagnado, 1998). We attempted to use tubulin

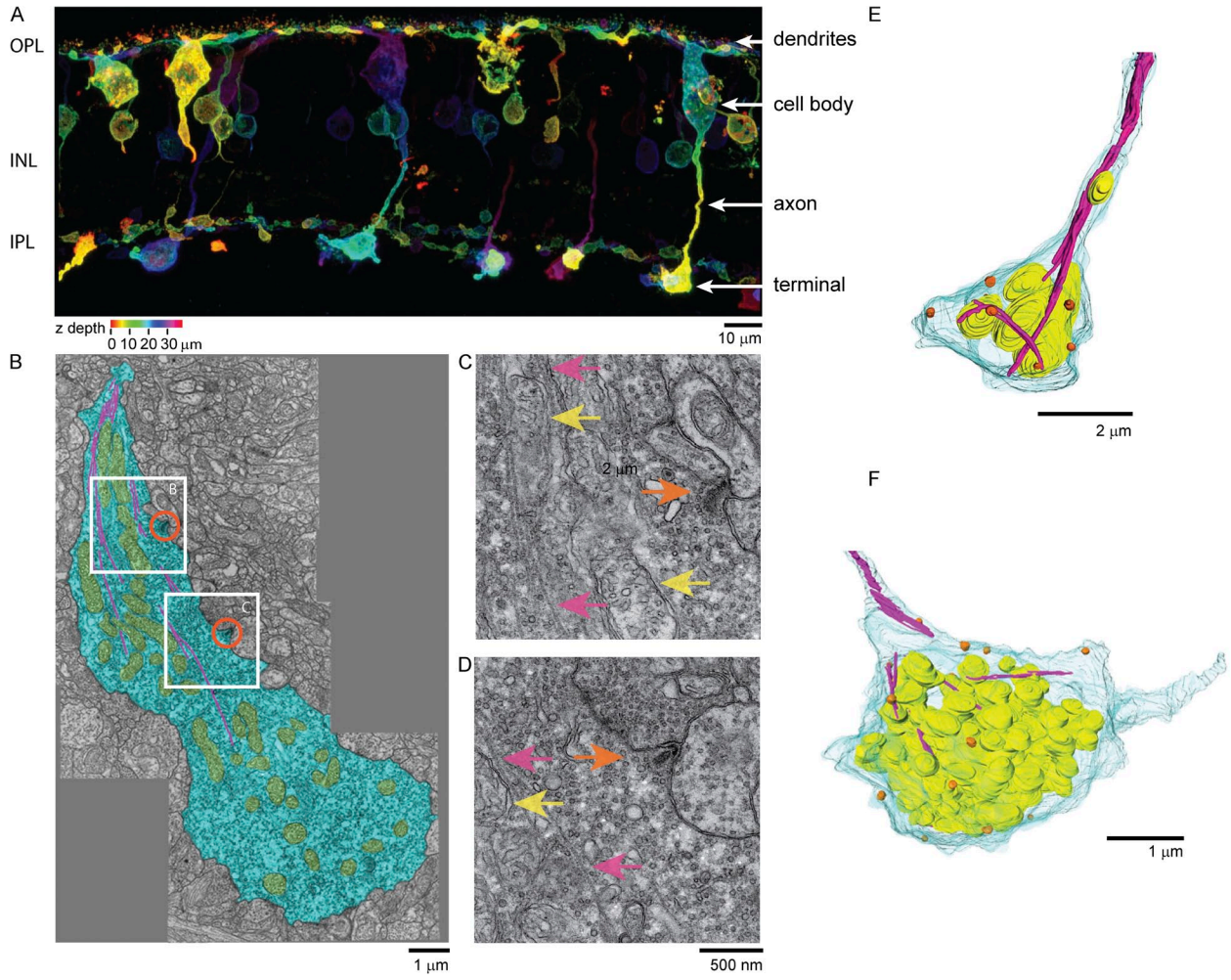

Figure 4. Subcellular structure of bipolar terminal imaged in intact retinal tissue slices. (A) PKC staining of cells in the outer plexiform layer (OPL), in the inner nuclear layer (INL), and in the inner plexiform layer (IPL) of the retina. Color code represents Z-height through the slice. (B) TEM image of a slice of the IPL of the goldfish retina. A single bipolar terminal (blue) contains an extensive network of mitochondria (yellow) and microtubules (magenta). Orange circles indicate two ribbon locations. (C) Magnified view of upper white box region shown in B. Orange arrows indicate ribbons. Magenta arrows indicate microtubules. Yellow arrows indicate mitochondria. (D) Magnified view of lower white box region shown in B. (E and F) 3-D reconstruction of 3-D serial block-face electron microscopy imaging of single bipolar terminal in the IPL. Blue, plasma membrane; yellow, mitochondria; orange, ribbons; magenta, microtubules.

and posttranslationally modified tubulin antibodies and SiR-tubulin live cell staining of microtubules in these slices, but the density of microtubules in the IPL was too high to clearly resolve individual cells above the intense fluorescence staining of the tissue. Thus, we turned to electron microscopy to investigate the structure of microtubules in the terminals of retinal bipolar cells in tissue. Fig. 4 B shows a single thin-section TEM image of the entire bipolar terminal located in the IPL. The diameter of the terminal in this section is 5.5 by 13 µm. Thousands of ∼40-nm diameter synaptic vesicles can be seen in this thin section, along with two oblong submicron-sized synaptic ribbons (Fig. 4 B, orange circles) and a network of mitochondria (Fig. 4 B, yellow structures). In several sections, we could clearly resolve ∼18-nm diameter hollow tubes corresponding to microtubules extending down from the axon shaft and traversing the length of the terminal (Fig. 4 B, magenta lines). Fig. 4 (C and D) shows magnified regions from Fig. 4 B where the microtubules (Fig. 4, C and D, pink arrows), mitochondria (Fig. 4, C and D, yellow arrows), and ribbons (Fig. 4, C and D, orange arrows) can be more clearly resolved. Similar to our fluorescence data in Fig. 1, we observed no clear association of microtubules with synaptic vesicles or ribbon structures.

The above TEM data were taken on single 65-nm-thick slices of the retina. To better understand how the entire terminal was organized, we used 3-D block-face serial SEM to create a full 3-D reconstruction of two bipolar cell terminals located in the IPL from hundreds of individual thin slices. Bipolar cells could be readily identified by their size, the presence of thousands of synaptic vesicles, and dozens of ribbon structures. Like that seen in the TEM images, we observed microtubules that originated from the axon and entered into the terminals (Fig. 4, E and F). In 3-D reconstructions, these microtubules were observed to traverse the diameter of the synaptic space and then proceed down the length of

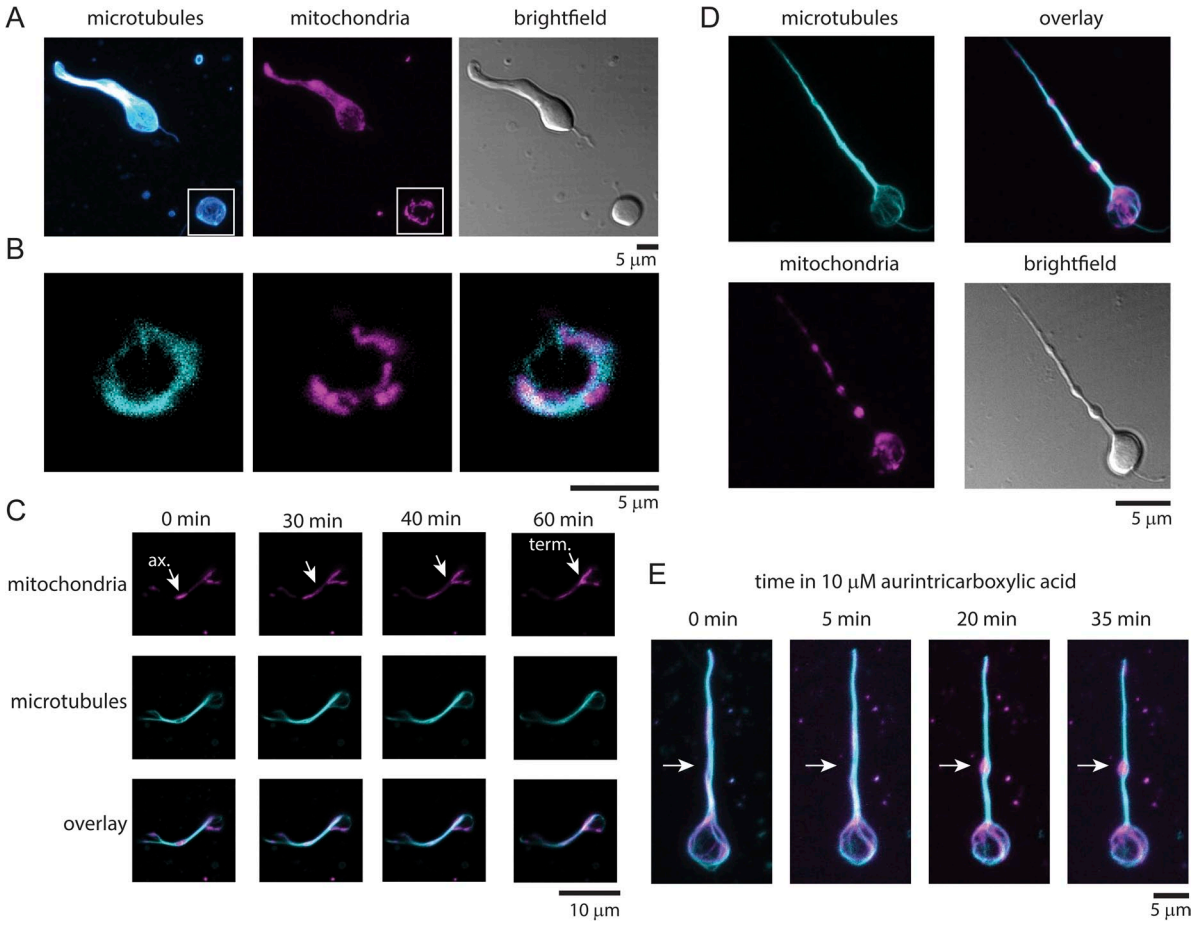

Figure 5. Mitochondria associate with the microtubule band in bipolar synaptic terminals. (A) 3-D max-intensity projection of a single live bipolar cell stained with SIR-tubulin and the mitochondrial marker TMRM. The white light image is shown to the right. (B) Magnified view of a single image plane from the 3-D image shown in A. The overlay image of these two regions is shown to the right. (C) Confocal time series of a mitochondrion moving in a bipolar axon and terminal over 1 h. Tubulin (cyan, SiR-tubulin) and mitochondria (magenta, TMRM) are stained as above. (D) Representative images of a bipolar axon and terminal stained for tubulin (cyan, SiR-tubulin) and mitochondria (magenta, TMRM) after a 20-min treatment with the kinesin inhibitor aurintricarboxylic acid. (E) Live cell image sequence of a single bipolar axon and terminal stained for tubulin (cyan, SiR-tubulin) and mitochondria (magenta, TMRM) after treatment with 10 µM of the kinesin inhibitor aurintricarboxylic acid. Time is referenced after the addition of drug.

the terminal. Because of the lower resolution and slicing of the block-face serial SEM, however, we could not always follow single microtubules through each continuous section. Each terminal, however, had many ribbons (13 ribbons, Fig. 4 E; 17 ribbons, Fig. 4 F) and a large collection of interconnected mitochondria, thousands of synaptic vesicles, and many microtubules. Occasionally, we observed single mitochondria in the axon shaft. These observations gave rise to the hypothesis that the microtubule structures observed in these cells act as transport tracks or anchoring structures for organelles such as mitochondria in the synaptic terminal (Sheng and Cai, 2012).

We directly tested this hypothesis by staining live cells with SiR-tubulin and the mitochondrial marker TMRM (Fig. 5, A and B). In terminals, we observed a colocalization between the marginal band of microtubules and mitochondria (Fig. 5 B). Quantitative analysis of the colocalization between these two structures in the synaptic terminals using a Pearson's correlation coefficient across the 3-D image stacks indicated substantial overlap between microtubules and mitochondria (average correlation coefficient, 0.56 ± 0.08, SD; n = 14 cells) (Larson et al., 2014). As shown in Fig. 1, substantial correlation was not seen in cells stained for microtubules and ribbons (average correlation coefficient, 0.09 ± 0.04, SD; n = 25 cells). In dual-stained living terminals, we occasionally observed mitochondria being transported along the axon into the terminal. Fig. 5 C shows mitochondria in the axon being stretched and pulled into the terminal over the course of 1 h. Transport of large organelles along oriented microtubules is thought to occur by kinesin motors. Inhibition of kinesin with the drug aurintricarboxylic acid has been shown to affect the behavior of the marginal band of microtubules in red blood cells (Diagouraga et al., 2014). Fig. 5 D shows that when bipolar cells were incubated with aurintricarboxylic acid for 20 min, distinct mitochondrial-filled swellings appeared in the axon of most bipolar cells in the culture (4.0 swellings/axon ± 0.3; n = 22 cells). Multiple large swellings were rarely seen in untreated cells (0.6 swellings/axon ± 0.2; n = 18 cells). The microtubule loop remained intact in the presence of drug. The formation of these axonal swellings could be followed over time directly in single terminals exposed to the drug (Fig. 5 E). These experiments demonstrate that mitochondria stall in the axon when kinesin activity is blocked. Collectively, our data indicate that the microtubule network of the axon is important for the supply of mitochondria into the synaptic terminal by kinesin motors.

DISCUSSION

Retinal bipolar cells contain giant synaptic terminals filled with upwards of a million synaptic vesicles. Dozens of electron-dense submicrometer-sized synaptic ribbons are thought to capture and organize a population of these vesicles to tune the functional output of these cells (Lagnado, 2003). Bipolar cells are constantly active and adjust their tonic release behavior according to inputs received from upstream photoreceptor cells. In this regard, the functional output of these cells is sometimes referred to as "analogue" (Lagnado, 2003). Neurons such as these have an extremely high and constant requirement for energy provided by ATP (Heidelberger, 1998; Harris et al., 2012). Activities including exocytosis, endocytosis, the loading of synaptic vesicles with neurotransmitters, maintenance of the membrane potential, calcium pumping, and ionic balances across organelles all require ATP (Harris et al., 2012). For example, previous work has shown that dialyzing nonhydrolyzable ATP analogues into bipolar terminals markedly slows endocytosis and the refilling of certain vesicle pools (Heidelberger et al., 2002). Furthermore, blockage of ATP-dependent calcium pumps at the plasma membrane causes major deficits in calcium handling in the terminal (Zenisek and Matthews, 2000). The ATP needed for these pumps is primarily generated by mitochondria (Zenisek and Matthews, 2000). Furthermore, in small mammalian synapses of the brain, ATP generated from mitochondria is critical for sustaining robust synaptic activity (Rangaraju et al., 2014). Here, we discover a marginal band of microtubules in retinal bipolar synaptic terminals that associates with mitochondria. We detected no association of ribbons with this structure. Changes in osmotic pressure, depolarization, and microtubule-depolymerizing drugs did not disrupt these microtubule structures. This suggests that they are a static structural component of these terminals. The movement of mitochondria between the cell body and the terminal, which is reliant on these microtubule tracks, is likely a key housekeeping and signaling property of these cells. Furthermore, streaming and bidirectional transport of other organelles are likely also driven by this microtubule-based process. Future work will be needed to determine the specific role that these spatially organized mitochondria play in the regulation of synaptic transmission in these large and continuously active neurons. For example, it is possible that individual ribbon synapses are regulated by the location of tethered mitochondria. Additionally, mitochondrial stress from turbulent mixing or mechanical strain in the terminal can damage mitochondria and lead to cell death as a result of released mitochondrial factors (Ji et al., 2012). The microtubule loop of bipolar cell terminals could be used to stabilize and protect mitochondria from damage in the dynamic cytoplasmic space of the terminal.

We observed that the disruption of kinesin motors induced the formation of mitochondria-filled varicosities in the axons of bipolar cells. Varicosities have been

observed in many neural systems (Kurshan et al., 2014). The formation of varicosities induced by the stalling of mitochondria might be important for the development of new synaptic connections along the axon in developing or plastic circuits. Bipolar cells in zebrafish have multiple synaptic terminals along their single axons with distinct signaling properties (Baden et al., 2014). The formation of these unique sites could be driven by the regulation of mitochondrial attachment to microtubules and the formation of varicosities.

Microtubules are critical organizers of cell shape, structure, and growth (Conde and Cáceres, 2009). They are essential to the extraordinary polarization that occurs between dendrites, the cell body, and axons of neurons. Microtubules have been detected in many synapses with imaging and biochemistry (Sheng and Cai, 2012; Wilhelm et al., 2014). Large loops of microtubules have been observed in other neuronal cell types. For example, in the Drosophila neuromuscular junction, microtubule loops form as new synaptic sites form on muscle (Roos et al., 2000). Disruption of these microtubule loops induces major changes in synaptic function in these systems. Microtubules have also been observed in mossy fiber synapses and other small synapses of the brain (Zhao et al., 2012). Furthermore, large extensive microtubule structures have been observed in the largest synapses of the mammalian brain—the Calyx of Held (Paysan et al., 2000). These studies demonstrate that prominent microtubule structures like those seen in goldfish bipolar cells likely have a fundamental signaling and structural role in many types of neurons. It will be interesting in the future to test if prominent microtubule–mitochondrial structures are also present in mammalian bipolar neurons, which have smaller and more branched synaptic terminals.

Importantly, we discovered a new organelle in the synaptic terminal of retinal bipolar cells. The microtubule structure was stable and contained significant posttranslational modifications. Large microtubule loops have been observed in other cells including red blood cells and in the Drosophila neuromuscular junction. It will be interesting to test if these microtubule–mitochondrial structures are a common component of other sensory neurons including hair cells and large mammalian synapses including the Calyx of Held and the mossy fiber synapse. The structural organization of these cells is driven by the underlying architecture of the cytoskeleton. The link between the cytoskeleton and the metabolic function of mitochondria is likely critical to the activity, regulation, and long-term health of these complex cells and tissues.

We would like to thank Pat Connelly and the NHLBI electron microscopy core for help with TEM. We would like to thank Richard Leapman of NIBIB and Guofeng Zhang of the NIBIB biomedical engineering and physical science shared resource for help with serial block-face SEM. We would like to thank Kai Johnsson (EPFL) for the kind gift of SiR-tublin and SiR-actin. We would like to thank Jeff Diamond, Kevin Briggman, and Jagesh Shah for helpful discussion; and the Taraska laboratory for critical reading of the manuscript.

J.W. Taraska is supported by the Intramural Research Program of the National Heart Lung and Blood Institute, National Institutes of Health (NIH). D. Zenisek is supported by a grant from the NIH (NIH EY014990).

The authors declare no competing financial interests.

Author contributions: M. Graffe and J.W. Taraska designed the experiments. M. Graffe performed the experiments. M. Graffe and J.W. Taraska analyzed the results. J.W. Taraska wrote the manuscript. D. Zenisek trained M. Graffe in retina preparation and gave experimental and systems advice. J.W. Taraska oversaw the project. All authors discussed the results and commented on the manuscript.

Sharona E. Gordon served as editor.

Submitted: 19 March 2015
Accepted: 28 May 2015

REFERENCES

Baden, T., A. Nikolaev, F. Esposti, E. Dreosti, B. Odermatt, and L. Lagnado. 2014. A synaptic mechanism for temporal filtering of visual signals. *PLoS Biol.* 12:e1001972. http://dx.doi.org/10.1371/journal.pbio.1001972

Behnke, O. 1970. A comparative study of microtubules of disk-shaped blood cells. *J. Ultrastruct. Res.* 31:61–75. http://dx.doi.org/10.1016/S0022-5320(70)90145-0

Conde, C., and A. Cáceres. 2009. Microtubule assembly, organization and dynamics in axons and dendrites. *Nat. Rev. Neurosci.* 10:319–332. http://dx.doi.org/10.1038/nrn2631

Diagouraga, B., A. Grichine, A. Fertin, J. Wang, S. Khochbin, and K. Sadoul. 2014. Motor-driven marginal band coiling promotes cell shape change during platelet activation. *J. Cell Biol.* 204:177–185. http://dx.doi.org/10.1083/jcb.201306085

Harris, J.J., R. Jolivet, and D. Attwell. 2012. Synaptic energy use and supply. *Neuron.* 75:762–777. http://dx.doi.org/10.1016/j.neuron.2012.08.019

Heidelberger, R. 1998. Adenosine triphosphate and the late steps in calcium-dependent exocytosis at a ribbon synapse. *J. Gen. Physiol.* 111:225–241. http://dx.doi.org/10.1085/jgp.111.2.225

Heidelberger, R., and G. Matthews. 1992. Calcium influx and calcium current in single synaptic terminals of goldfish retinal bipolar neurons. *J. Physiol.* 447:235–256. http://dx.doi.org/10.1113/jphysiol.1992.sp019000

Heidelberger, R., P. Sterling, and G. Matthews. 2002. Roles of ATP in depletion and replenishment of the releasable pool of synaptic vesicles. *J. Neurophysiol.* 88:98–106.

Holt, M., A. Cooke, A. Neef, and L. Lagnado. 2004. High mobility of vesicles supports continuous exocytosis at a ribbon synapse. *Curr. Biol.* 14:173–183. http://dx.doi.org/10.1016/j.cub.2003.12.053

Ji, J., Y.Y. Tyurina, M. Tang, W. Feng, D.B. Stolz, R.S. Clark, D.F. Meaney, P.M. Kochanek, V.E. Kagan, and H. Bayır. 2012. Mitochondrial injury after mechanical stretch of cortical neurons in vitro: Biomarkers of apoptosis and selective peroxidation of anionic phospholipids. *J. Neurotrauma.* 29:776–788. http://dx.doi.org/10.1089/neu.2010.1602

Job, C., and L. Lagnado. 1998. Calcium and protein kinase C regulate the actin cytoskeleton in the synaptic terminal of retinal bipolar cells. *J. Cell Biol.* 143:1661–1672. http://dx.doi.org/10.1083/jcb.143.6.1661

Kremer, J.R., D.N. Mastronarde, and J.R. McIntosh. 1996. Computer visualization of three-dimensional image data using IMOD. *J. Struct. Biol.* 116:71–76.

Kurshan, P.T., A.Q. Phan, G.J. Wang, M.M. Crane, H. Lu, and K. Shen. 2014. Regulation of synaptic extracellular matrix composition is critical for proper synapse morphology. *J. Neurosci.* 34:12678–12689. http://dx.doi.org/10.1523/JNEUROSCI.1183-14.2014

Lagnado, L. 2003. Ribbon synapses. *Curr. Biol.* 13:R631. http://dx.doi.org/10.1016/S0960-9822(03)00566-9

Lagnado, L., A. Gomis, and C. Job. 1996. Continuous vesicle cycling in the synaptic terminal of retinal bipolar cells. *Neuron.* 17:957–967. http://dx.doi.org/10.1016/S0896-6273(00)80226-3

Larson, B.T., K.A. Sochacki, J.M. Kindem, and J.W. Taraska. 2014. Systematic spatial mapping of proteins at exocytic and endocytic structures. *Mol. Biol. Cell.* 25:2084–2093. http://dx.doi.org/10.1091/mbc.E14-02-0771

Lazarides, E. 1987. From genes to structural morphogenesis: The genesis and epigenesis of a red blood cell. *Cell.* 51:345–356. http://dx.doi.org/10.1016/0092-8674(87)90631-3

Lukinavičius, G., L. Reymond, E. D'Este, A. Masharina, F. Göttfert, H. Ta, A. Güther, M. Fournier, S. Rizzo, H. Waldmann, et al. 2014. Fluorogenic probes for live-cell imaging of the cytoskeleton. *Nat. Methods.* 11:731–733. http://dx.doi.org/10.1038/nmeth.2972

Magiera, M.M., and C. Janke. 2014. Post-translational modifications of tubulin. *Curr. Biol.* 24:R351–R354. http://dx.doi.org/10.1016/j.cub.2014.03.032

Masland, R.H. 2012. The neuronal organization of the retina. *Neuron.* 76:266–280. http://dx.doi.org/10.1016/j.neuron.2012.10.002

Matthews, G., and P. Fuchs. 2010. The diverse roles of ribbon synapses in sensory neurotransmission. *Nat. Rev. Neurosci.* 11:812–822. http://dx.doi.org/10.1038/nrn2924

Paysan, J., W.G. Conroy, J.S. Coggan, and D.K. Berg. 2000. The neurofilament infrastructure of a developing presynaptic calyx. *J. Comp. Neurol.* 425:284–294. http://dx.doi.org/10.1002/1096-9861(20000918)425:2<284::AID-CNE10>3.0.CO;2-N

Pfeifer, C.R., A. Shomorony, M.A. Aronova, G. Zhang, T. Cai, H. Xu, A.L. Notkins, and R.D. Leapman. 2015. Quantitative analysis of mouse pancreatic islet architecture by serial block-face SEM. *J. Struct. Biol.* 189:44–52. http://dx.doi.org/10.1016/j.jsb.2014.10.013

Rangaraju, V., N. Calloway, and T.A. Ryan. 2014. Activity-driven local ATP synthesis is required for synaptic function. *Cell.* 156:825–835. http://dx.doi.org/10.1016/j.cell.2013.12.042

Roos, J., T. Hummel, N. Ng, C. Klämbt, and G.W. Davis. 2000. *Drosophila* Futsch regulates synaptic microtubule organization and is necessary for synaptic growth. *Neuron.* 26:371–382. http://dx.doi.org/10.1016/S0896-6273(00)81170-8

Schmitz, F., A. Königstorfer, and T.C. Südhof. 2000. RIBEYE, a component of synaptic ribbons: A protein's journey through evolution provides insight into synaptic ribbon function. *Neuron.* 28:857–872. http://dx.doi.org/10.1016/S0896-6273(00)00159-8

Sheng, Z.H., and Q. Cai. 2012. Mitochondrial transport in neurons: impact on synaptic homeostasis and neurodegeneration. *Nat. Rev. Neurosci.* 13:77–93.

Stell, W.K. 1967. The structure and relationships of horizontal cells and photoreceptor-bipolar synaptic complexes in goldfish retina. *Am. J. Anat.* 121:401–423. http://dx.doi.org/10.1002/aja.1001210213

Tachibana, M., and A. Kaneko. 1987. gamma-Aminobutyric acid exerts a local inhibitory action on the axon terminal of bipolar cells: evidence for negative feedback from amacrine cells. *Proc. Natl. Acad. Sci. USA.* 84:3501–3505. http://dx.doi.org/10.1073/pnas.84.10.3501

von Gersdorff, H., E. Vardi, G. Matthews, and P. Sterling. 1996. Evidence that vesicles on the synaptic ribbon of retinal bipolar neurons can be rapidly released. *Neuron.* 16:1221–1227. http://dx.doi.org/10.1016/S0896-6273(00)80148-8

von Gersdorff, H., T. Sakaba, K. Berglund, and M. Tachibana. 1998. Submillisecond kinetics of glutamate release from a sensory synapse. *Neuron.* 21:1177–1188. http://dx.doi.org/10.1016/S0896-6273(00)80634-0

Wilhelm, B.G., S. Mandad, S. Truckenbrodt, K. Kröhnert, C. Schäfer, B. Rammner, S.J. Koo, G.A. Claßen, M. Krauss, V. Haucke, et al. 2014. Composition of isolated synaptic boutons reveals the amounts of vesicle trafficking proteins. *Science.* 344:1023–1028. http://dx.doi.org/10.1126/science.1252884

Zenisek, D., and G. Matthews. 2000. The role of mitochondria in presynaptic calcium handling at a ribbon synapse. *Neuron.* 25:229–237. http://dx.doi.org/10.1016/S0896-6273(00)80885-5

Zenisek, D., J.A. Steyer, and W. Almers. 2000. Transport, capture and exocytosis of single synaptic vesicles at active zones. *Nature.* 406:849–854. http://dx.doi.org/10.1038/35022500

Zenisek, D., N.K. Horst, C. Merrifield, P. Sterling, and G. Matthews. 2004. Visualizing synaptic ribbons in the living cell. *J. Neurosci.* 24:9752–9759. http://dx.doi.org/10.1523/JNEUROSCI.2886-04.2004

Zhao, S., D. Studer, X. Chai, W. Graber, N. Brose, S. Nestel, C. Young, E.P. Rodriguez, K. Saetzler, and M. Frotscher. 2012. Structural plasticity of hippocampal mossy fiber synapses as revealed by high-pressure freezing. *J. Comp. Neurol.* 520:2340–2351. http://dx.doi.org/10.1002/cne.23040